Applied Surface Science xxx (2017) xxx–xxx

Contents lists available at ScienceDirect

Applied Surface Science

journal homepage: www.elsevier.com/locate/apsusc

Full Length Article

Visible-light-driven N-$(BiO)_2CO_3$/Graphene oxide composites with improved photocatalytic activity and selectivity for NO_x removal

Meijuan Chen [a], Yu Huang [b,c,*], Jie Yao [b], Jun-ji Cao [b,c], Yuan Liu [b]

[a] School of Human Settlements and Civil Engineering, Xi'an Jiaotong University, Xi'an 710049, China
[b] Key Lab of Aerosol Chemistry & Physics, Institute of Earth Environment, Chinese Academy of Sciences, Xi'an 710061, China
[c] State Key Lab of Loess and Quaternary Geology (SKLLQG), Institute of Earth Environment, Chinese Academy of Sciences, Xi'an 710061, China

ARTICLE INFO

Article history:
Received 16 February 2017
Received in revised form 15 May 2017
Accepted 5 June 2017
Available online xxx

Keywords:
$(BiO)_2CO_3$
N doping
GO
NO removal
Composite

ABSTRACT

N-doped $(BiO)_2CO_3$ (NBOC)/graphene oxide (GO) composite obtained from three-dimensional hierarchical microspheres is successfully synthesized by one-pot hydrothermal method for the first time. In this synthesis, citrate ion plays a critical role in N doping. The obtained samples are used to degrade gaseous nitrogen oxides (NO_x) at parts-per-billion (ppb) level under visible-light irradiation. NBOC–GO composite with 1.0 wt% graphene oxide (GO) displays the highest photocatalytic NO removal efficiency, which is 4.3 times higher than that of pristine $(BiO)_2CO_3$. Moreover, NBOC–GO composite significantly inhibits toxic NO_2 intermediate production, indicating its high selectivity for NO conversion. Compared with regular GO, N doping considerably improves the catalytic performance of NBOC–GO composite, which increases NO removal by 74.6% and fully inhibits NO_2 generation. The improved photocatalytic activity is mainly ascribed to extended optical absorption ability and enhanced separation efficiency of photogenerated charge carriers over NBOC–GO composite. Both results of electron spin resonance and theoretical analysis of band structure indicate that NO removal is dominated by oxidation with $^{\bullet}OH$ and $^{\bullet}O_2^-$ radicals. The photocatalytic activity improvement mechanism over the NBOC–GO composite is proposed accordingly based on systematic characterizations. This study demonstrates a feasible route to fabricating Bi-containing composites with high selectivity and stability for air pollution control and provides a new insight into the associated photocatalytic mechanisms.

1. Introduction

Nitrogen oxides (NO_x, the sum of NO and NO_2) are considered as some of the most important precursors for secondary organic aerosol (SOA) formation, which significantly contributes to $PM_{2.5}$ mass concentration [1]. In Europe and North America, NO_x emissions from fossil fuel consumption are decreasing; however, in China, the increasing consumption of fossil fuels and biomass results in increased NO_x emissions, especially in urban and industrial areas [2]. To reduce the adverse effects of emissions on human health and environmental protection [3], the development of efficient strategies to remove NO_x from the atmosphere is of considerable importance [4]. Currently, the most commonly adopted NO_x control technology is selective catalytic reduction using ammonia. However, this method is only applicable for NO_x with high concentration (hundreds of ppm) at high temperature [5]. Thereby, semiconductor photocatalysis has received intensive attention in recent years as an alternative strategy for NO_x decomposition at parts-per-billion (ppb) levels at ambient temperature [6].

Recently, a series of Bi-containing photocatalysts has been developed owing to their excellent photocatalytic activity during environmental pollutant removal. In particular, aurivillius bismuth subcarbonate ($(BiO)_2CO_3$), composed of $(Bi_2O_2)^{2+}$ and CO_3^{2-} layers, shows promising UV light-activated photocatalytic activity. However, the application of pristine $(BiO)_2CO_3$ (E_g = 3.1–3.5 eV) is hindered by the relatively low utilization efficiency of visible light and rapid recombination rate of photogenerated charge carriers [7,8]. Considering that visible light accounts for 46% of the total solar light energy, exploring photocatalytic materials with visible light absorption ability is highly desirable. Various approaches, such as noble metal deposition and element doping, have been utilized to improve the visible light utilization efficiency of $(BiO)_2CO_3$ [9,10]. For instance, Ag/$(BiO)_2CO_3$ was reported to exhibit improved visible light photocatalytic activity because of the significant sur-

* Corresponding author at: Key Lab of Aerosol Chemistry & Physics, Institute of Earth Environment, Chinese Academy of Sciences, Xi'an 710061, China.
E-mail address: huangyu@ieecas.cn (Y. Huang).

http://dx.doi.org/10.1016/j.apsusc.2017.06.056
0169-4332/

face plasmon resonance effect induced by Ag loading [8]. Huang et. al found that the N-doped $(BiO)_2CO_3$ demonstrated superior visible light activity compared with pure $(BiO)_2CO_3$ because the dopant narrows the band gap, thereby allowing intensive use of visible light [11]. Apart from improving visible light utilization, the control of e^-/h^+ recombination rate over $(BiO)_2CO_3$ is also a crucial issue. Graphene oxide (GO), as the cousin of graphene, has attracted considerable attention due to its unique properties, such as high charge carrier mobility at room temperature, large specific surface area, extraordinary conductivity, and excellent optical transparency [12]. Owing to the presence of numerous delocalized electrons in the conjugated carbon network, GO is one of the most ideal supports for photocatalysts that can facilitate photogenerated electron separation and migration. For example, Puttaswamy et al. synthesized a hierarchical GO/$(BiO)_2CO_3$ composite that showed improved photocatalytic activity on RhB degradation [13]. However, approaches aiming to simultaneously overcome these two aspects of drawbacks, namely, low visible light utilization and rapid e^-/h^+ recombination, are scarce. In this study, N-doped $(BiO)_2CO_3$/graphene oxide (NBOC–GO) composites are synthesized to obtain high photocatalytic performance on NO removal by providing synchronously high visible light utilization efficiency and low e^-/h^+ recombination.

During the photocatalytic process for NO decomposition, the chemical reactions between NO and photogenerated reactive radicals can produce NO_2 intermediates and NO_3^- as final products. However, the yield of NO_2 gas in the system is not favorable because of its intensive corrosion and toxicity, which makes it considerably harmful than NO [14]. Dong et al. reported that the NO_2 generation was extremely higher over pure $(BiO)_2CO_3$, accounting for 28% of the degraded NO ($\frac{\Delta C_{NO2}}{\Delta C_{NO}} \times 100\%$) [8]. As far as we know, few literatures have reported on $(BiO)_2CO_3$-based photocatalysts with high selectivity on NO removal to suppress NO_2 generation.

In this study, NBOC–GO composites are prepared using a one-pot hydrothermal method and are then used to degrade gaseous NO at a parts-per-billion (ppb) level under visible light. The as-prepared NBOC–GO composites present excellent NO removal efficiency and ignorable NO_2 generation. The effect of GO/NBOC weight ratios are investigated to obtain the optimum formula. We systematically characterize the obtained NBOC–GO sample and discuss the mechanisms of its enhanced photocatalytic activity. Furthermore, the contributions of N doping and GO coupling on photocatalytic activity enhancement are quantitatively and qualitatively determined.

2. Experimental

2.1. Materials

Bismuth citrate ($C_6H_5BiO_7$), bismuth nitrate ($Bi(NO_3)_3$), and urea ($CO(NH_2)_2$) were obtained from Evonik Degussa (Shanghai, China). Graphite powder, sulfuric acid (H_2SO_4, 98%), hydrochloric acid (HCl, 36.0%–38.0%), hydrogen peroxide (H_2O_2), sodium hydrate (NaOH), and potassium permanganate ($KMnO_4$) were purchased from Sigma–Aldrich (USA).

2.2. Synthesis of NBOC–GO composites

First, GO was synthesized based on a modified Hummer's method. Briefly, 1.0 g graphite powder was dispersed into 23 mL H_2SO_4 at room temperature by stirring for 8 h. Subsequently, the container (flask) was cooled to 0 °C using an ice bath. Afterward, 3.0 g $KMnO_4$ was slowly added to the above mixture. The final suspension was heated to 35 °C for 30 min and then to 65–80 °C for 45 min to obtain a dark brown paste. Subsequently, the paste was diluted with 46 mL deionized (DI) water at 95–105 °C. Exactly 10 mL 30% H_2O_2 was then slowly added to react with the residual $KMnO_4$. The resulting suspension was centrifuged, washed with DI water, and dried at 80 °C to obtain GO powder.

Second, 2 mmol bismuth citrate and 5 mmol urea were dissolved in 35 mL DI water through vigorous magnetic stirring with the addition of a certain GO amount. The suspension was subsequently transferred into a Teflon-lined stainless steel autoclave and kept at 160 °C for 24 h. The precipitate was collected from the autoclave via filtration, washed with DI water and ethanol in sequence, and dried at 80 °C. The obtained powder was the NBOC–GO sample. To investigate the effect of GO/NBOC weight ratios, the initial GO amounts were set at 0.1, 0.5, 1.0, and 1.5 wt% of NBOC, which were indexed as NBOC–GO 0.1, NBOC–GO 0.5, NBOC–GO 1.0, and NBOC–GO 1.5, respectively. The NBOC sample was prepared using the same procedure except GO addition.

For comparison, the pure $(BiO)_2CO_3$ (BOC) sample was synthesized by replacing bismuth citrate with bismuth nitrate. Other approaches are similar to those of NBOC. The BOC-GO 1.0 composite was synthesized as a dispersing GO powder (containing 1.0 wt% BOC) into the precursor solution for BOC synthesis.

2.3. Characterization

The phase structures of the catalysts were recorded on a Philips X'Pert Pro Super diffractometer using Cu Kα (λ = 0.154 nm) radiation. Raman spectroscopy was carried out using a Renishaw inVia Raman System 1000 spectrometer. Fourier transform infrared spectrometer (Magna-IR 50, Nicolet, USA) was used to test the Fourier transform infrared spectroscopy (FTIR) spectra. The UV–vis reflectance spectra was obtained from a Varian Cary 100 Scan UV–vis system. X-ray photoelectron spectroscopy (XPS) was performed on a Quantum 2000 Scanning ESCA Microprobe. The sample morphology was characterized using scanning electron microscopy (SEM, SUPRA 55, Japan) and transmission electron microscopy (TEM, JEM-2010, Japan), respectively. The photoluminescence (PL) spectra of samples were tested with a PL spectrometer (PE, LS-55, USA) at 280 nm excitation wavelength. The N_2 adsorption/desorption isotherms were characterized using Brunner–Emmet–Teller (BET) measurement analyzer (Micromeritics Instrument, ASAP 2020, USA). To determine the $^{\bullet}OH$ and $^{\bullet}O_2^-$ radical formation, electron spin resonance (ESR) were conducted on an ER200-SRC spectroscopy (Bruker, Germany). The ESR test samples were prepared by dispersing 0.05 g NBOC–GO into 25 mM 5, 5′-dimethyl-1-pirroline-N-oxide (DMPO) solution for DMPO–$^{\bullet}OH$ or 50 mL methanol dispersion for DMPO–$^{\bullet}O_2^-$. The photoelectrochemical properties of the samples were tested using an electrochemical workstation (PARSTAT 4000, USA). The photocurrent–time curve was measured at a voltage of 0.2 V in a 0.5 M Na_2SO_4 electrolyte. Electrochemical impedance spectroscopy (EIS) was investigated at 5 mV voltage amplitude with a frequency range of 0.1–100 kHz under an open-circuit voltage. The flat band potential of sample was measured through Mott–Schottky measurement at a frequency of 1000 Hz in 0.1 mol L^{-1} Na_2SO_4 aqueous solution (pH = 7.0).

2.4. Photocatalytic activity test

To test the photocatalytic activity, the air pollutant NO was chosen as the probe to examine the photocatalyst performance. The NO gas continuously flows into a rectangular reactor made of stainless steel with a dimension of 10 (height) × 30 (length) × 15 cm (width). A Saint-Glass was covered on top of the rectangular reactor to allow passage of light. Exactly 0.2 g catalyst was dispersed on a sample dish placed on the center of the reactor. The sample dish was prepared by coating the catalyst onto a dish with 12.0 cm diameter.

Please cite this article in press as: M. Chen, et al., Visible-light-driven N-$(BiO)_2CO_3$/Graphene oxide composites with improved photocatalytic activity and selectivity for NO_x removal, Appl. Surf. Sci. (2017), http://dx.doi.org/10.1016/j.apsusc.2017.06.056

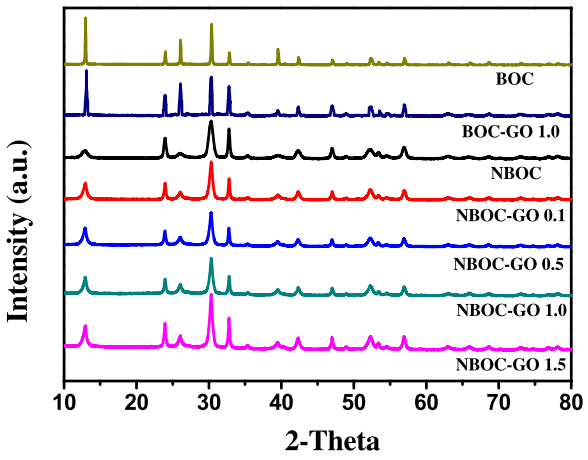

Fig. 1. XRD patterns of BOC, BOC–GO 1.0, NBOC and NBOC–GO composites.

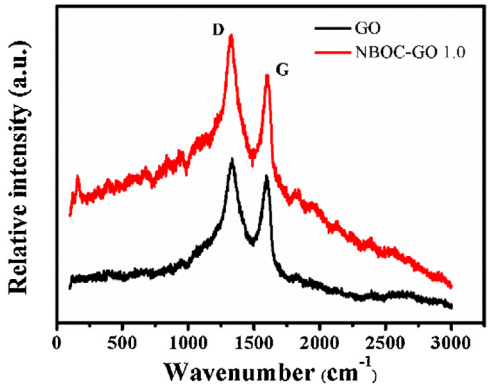

Fig. 2. Raman spectra of GO and NBOC–GO 1.0 composites.

The NO gas was supplied by a compressed gas cylinder and diluted with N_2 gas. The NO concentration in the cylinder was 48 ppm and diluted to 400 ppb for photocatalytic activity testing using a zero air generator (Sabio 4010, USA). When an equilibrium was achieved following the adsorption/desorption between the catalyst and NO gas, the Xenon lamp (300 W, PLS-SXE 300, Beijing) was turned on to start the photocatalytic reaction. The light irradiation from the Xenon lamp was regarded as the simulated solar light. The NO and NO_2 concentrations were continuously measured during the reaction.

3. Results and discussion

3.1. Phase structure and chemical compositions of the as-prepared samples

Fig. 1 shows the XRD patterns of BOC, BOC-GO 1.0, NBOC and NBOC–GO samples. All samples show similar XRD patterns, which can be indexed to tetragonal $(BiO)_2CO_3$ with JCPDS no. 41-1488. Compared with pure $(BiO)_2CO_3$, NBOC has significantly broadened peaks withlattice distortion resulting from lower crystallinity owing to the presence of nitrogen [15]. The consistent phase structure between NBOC and NBOC–GO confirms that the crystal structure of N-doped $(BiO)_2CO_3$ was not changed during the NBOC–GO synthesis process.

Raman spectroscopy is performed to verify the presence of GO in the NBOC–GO 1.0 composite. Fig. 2 presents the results. The 1610 and 1326 cm^{-1} Raman bands are observed in both samples, which should be attributed to the G and D bands of GO, respectively [16]. Moreover, the I_D/I_G intensity ratio is an indicator of the disorder degree, where I_D and I_G are the intensities of D and G bands, respectively [16]. Higher I_D/I_G value represents higher disorder and more defects because the D band is relative to the disorder and defects in the hexagonal graphitic layers. The imperceptible change in I_D/I_G ratio between GO (1.09) and NBOC–GO 1.0 (1.12) indicates that GO is formed through a nondestructive coalescent approach in the NBOC–GO composites. Differently, a characteristic band at 162 cm^{-1} is observed in the NBOC–GO 1.0 composite alone, which is attributed to the external vibration of carbonate ion (CO_3^{2-}) [17].

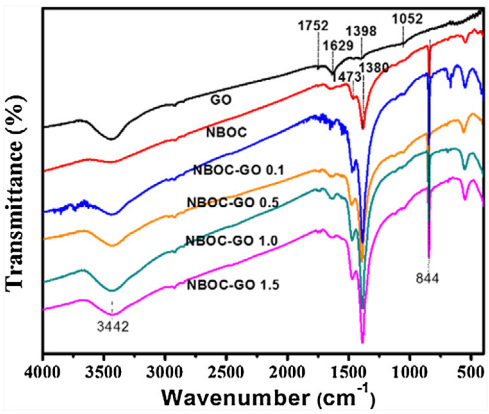

Fig. 3. FTIR spectra of as-prepared GO, NBOC, NBOC–GO samples.

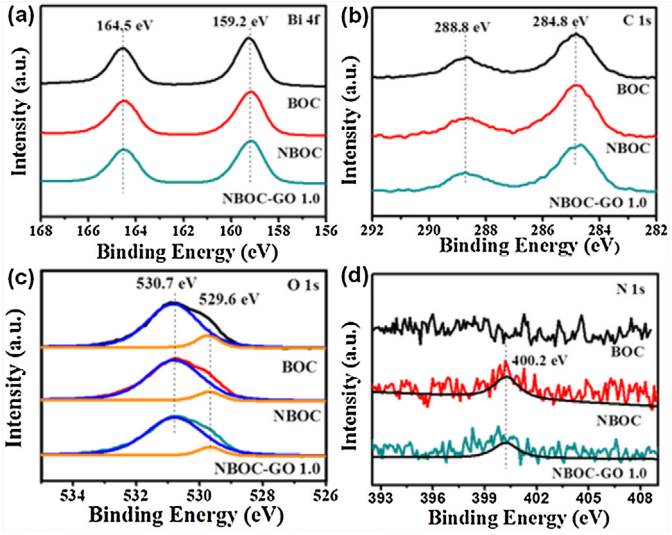

Fig. 4. XPS spectra of BOC, NBOC and NBOC–GO 1.0 samples.

Fig. 3 illustrates the FTIR images of GO, NBOC, and NBOC–GO composites (0.1, 0.5, 1.0, and 1.5). For GO sample, four adsorption peaks are observed at 1752, 1629, 1398, and 1052 cm^{-1}. The peak at 1752 cm^{-1} is attributed to C=O stretching vibration in the carboxyl group. The absorption peak at 1629 cm^{-1} indicates an O—H bending vibration in the epoxide functional group. The peaks at 1398 and 1052 cm^{-1} result from the vibrations of carboxyl C—O and alkoxy C—O stretching, respectively [15,18]. For the NOBC FTIR spectra, the CO_3^{2-} characteristic band groups ion, including ν_3 (1473 and 1380 cm^{-1}) and ν_2 (844 cm^{-1}) vibrational modes, are observed [15]. For all NBOC–GO samples, the characteristic bands of both NBOC and GO still remain, suggesting successful NBOC–GO composite formation in the samples. Moreover, the broad band in 3442 cm^{-1} is found in all the samples, which is caused by the physically absorbed H_2O from the atmosphere.

XPS measurement is conducted to identify the elements in BOC, NBOC, and NBOC–GO 1.0 samples. In Fig. 4a, the Bi peaks at 159.2

Please cite this article in press as: M. Chen, et al., Visible-light-driven N-$(BiO)_2CO_3$/Graphene oxide composites with improved photocatalytic activity and selectivity for NO_x removal, Appl. Surf. Sci. (2017), http://dx.doi.org/10.1016/j.apsusc.2017.06.056

and 164.5 eV correspond to Bi $4f_{7/2}$ and Bi $4f_{5/2}$, respectively. In Fig. 4b, the C 1s peaks at 284.8 and 288.8 eV are attributed to the carbon in carbonate group. The O 1s spectra located at 530.7 and 529.6 eV, as shown in Fig. 4c, are caused by O–Bi and hydroxyl species, respectively, where the hydroxyl species originated from the absorbed H_2O on the catalyst surface from the atmosphere [15]. It is worth noting that the N 1s peak (Fig. 4d) at 400.2 eV is present in NBOC and NBOC–GO 1.0 samples but absent in BOC sample. This observation indicates successful N doping in NBOC and NBOC–GO 1.0 samples. Moreover, the surface atomic nitrogen concentration is found to be 0.83% based on the XPS result of NBOC. From the raw material used for NBOC synthesis (i.e., $C_6H_5BiO_7$ and $CO(NH_2)_2$), the N element in NBOC should be attributed to the urea. However, the N element is absent in BOC sample that utilized $Bi(NO_3)_3$ as the Bi source. This finding suggests that citrate ion in bismuth citrate plays an important role in nitrogen doping.

3.2. Morphology

SEM and TEM analyses were adopted to characterize the size and morphology of the as-prepared samples (Fig. 5). As shown in Fig. S1, the pure BOC is composed of nanoplates. The NBOC consisted of a large number of nanoplates as shown in Fig. 5a. Fig. 5b reveals a thickness of the nanoplates of approximately 129.6–213.0 nm. In Fig. 5c, the NBOC–GO 1.0 consisted of three-dimensional flower-like hierarchical microspheres, wherein the flower is self-assembled from two-dimensional nanosheets. Obviously, few un-assembled nanosheets disperse in the NBOC–GO sample. The close-up view of NBOC–GO shows that the thickness of the nanosheets is approximately 14.2–32.3 nm (Fig. 5d). The thickness of nanosheets in NBOC–GO composite is much smaller than that of pure NBOC, which might be due to that the GO template is thin. The thin nanosheets would enhance the photocatalytic performance by providing increased exposure surface and facilitating the mobility of charge carriers, such as ZnO–GO composite and $BiVO_4$ nanosheets [19,20].

The morphology of NBOC–GO is further confirmed by TEM image (Fig. 6a). As shown in Fig. S2, GO is composed of thin, transparent gauze-like sheets [21]. The two-dimensional nanosheets in Fig. 6a were obviously originated from GO, whereas the nanoparticles and some dispersed nanosheets with small size should be ascribed to the N-$Bi_2O_2CO_3$. Therefore, the NBOC nanosheets in the NBOC–GO composite are assembled of nanoparticles (Fig. 6a). This condition suggests that the appearance of GO in the reaction precursor changes the morphology of NBOC, wherein the GO acts as the template, supporting NBOC nanoparticle growth into nanosheets on the GO and then assembled as hierarchical flower. Similar finding has been reported by Xu et al., wherein Ag_2CrO_4 semiconductor changed from bulk to small nanoparticles after dosing GO into the precursor solution [22]. The corresponding high-resolution transmission electron microscopy (HRTEM) image (Fig. 6b) shows that the lattice fringe is ca. 0.273 nm, corresponding to the (110) crystal plane of tetragonal phase NBOC. The selected-area electron diffraction (SEAD) pattern in the inset of Fig. 6b shows clear diffraction rings, suggesting that the NBOC is a polycrystalline structure. The inner two diffraction rings correspond to (110) and (020) planes of $Bi_2O_2CO_3$. The phase analysis from HRTEM and SEAD images confirms the tetragonal phase structure analyzed from XRD, demonstrating that NBOC has successfully anchored to the surface of the GO sheets.

3.3. Optical absorption and surface areas

Fig. 7a displays the UV–vis diffuse reflectance spectra of the as-prepared samples. A sharp absorption edge is observed at 400 nm for pure BOC sample. After doping with N, the absorption edge shifts to 600 nm in NBOC sample, indicating that the N doping tailors the absorption spectrum from UV to visible ranges. Compared with NBOC, the optical absorption intensities of all NBOC–GO samples are strengthened in the range of 600–900 nm. Moreover, the absorption edge of NBOC–GO samples exhibit no significant shift compared with NBOC. The differences between NBOC-GO and NBOC should be ascribed to the presence of GO. These findings suggest that the GO in the NBOC–GO composites consist of free carbon rather than incorporated carbon since the free carbon leads to a broad background absorption in the visible-light region, whereas incorporated carbon results in the change of adsorption edge [19]. Moreover, the absorption intensities in 600–900 nm are gradually increased as the GO content increased. This finding implies that the higher the GO content, the more efficient the utilization of solar energy. This observation is consistent with the color change among the NBOC–GO composites, which turns from light yellow to brown with the increment of GO content (Fig. 7a). Additionally, compared with BOC, the BOC-GO 1.0 shows a significant enhancement in optical absorption at visible light range, while the adsorption edge does not shift. This observation is agreement with changes from NBOC to NBOC-GO.

The band gaps of BOC and NBOC are calculated to be 3.26 and 2.94 eV by using the Kubelka–Munk function, respectively, which are estimated from the intercept of the tangent by plotting $(\alpha h\nu)^{1/2}$ vs. $h\nu$ as shown in Fig. 7b [23]. The abbreviations α and $h\nu$ represent the absorption coefficient and photon energy, respectively.

Table 1 shows the BET specific surface area (S_{BET}) of the BOC, BOC–GO 1.0, NBOC and NBOC–GO composites. The BET specific surface area of NBOC reaches 25.31 m^2/g, which is 10.9 times of BOC. However, after coupling with GO, the S_{BET} of NBOC–GO is almost unchanged as compared with NBOC. This observation suggests that N doping in the NBOC-GO composites contributes to the more significant improvement on the S_{BET} than the approach of coupling with GO. Differently, S_{BET} of the BOC–GO composites increases slightly from 2.32 m^2/g to 5.47 m^2/g when the GO content changes from 0 wt.% to 1.0 wt.%, which is because the GO with a large S_{BET} can act as support for the BOC growth, leading to the formation of a larger S_{BET} in the BOC–GO 1.0 composite [19]. In general, the large S_{BET} benefits the photocatalytic performance by providing more active sites for the pollutants and promoting the e^-–h^+ pairs separation [24].

3.4. Photocatalytic activity evaluation

The photocatalytic activity of the as-prepared samples is examined for NO removal under visible-light irradiation. Fig. 8a depicts the remaining NO ($\frac{C_{NO}}{C_0\ of\ NO} \times 100\%$) vs. irradiation time over BOC, BOC–GO 1.0, NBOC, and NBOC–GO composites. The BOC sample shows the lowest NO removal efficiency of 11.8%. By contrast, the NBOC presents a significant improvement in NO removal with a removal efficiency of 40.6%. All NBOC–GO (0.1, 0.5, 1.0, and 1.5) samples show better NO removal performance than pure NBOC. The optimum NO removal efficiency is 50.4% as the GO amount increases to 1.0%, which is 4.3 times of pure $(BiO)_2CO_3$. However, the further increase of GO amount results in the impairment on NO removal, showing a decreased removal efficiency of 47.0% at NBOC–GO 1.5 composite. Therefore, an unlimited increase of GO amount does not guarantee a beneficial effect on the photocatalytic performance because the overdosed GO would hinder the light absorption of NBOC. NBOC (40.6%) shows better NO removal efficiency than BOC–GO 1.0 (21.3%), suggesting that N doping plays a more important role than GO on the improvement of the photocatalytic activity. N doping contributes to 74.6% of the improvement in NO removal $\left(\frac{NBOC-BOC}{NBOC-GO1.0composite-BOC}\right)$ and the GO responses for the minor 25.4% in the NBOC–GO 1.0 sample.

Please cite this article in press as: M. Chen, et al., Visible-light-driven N-$(BiO)_2CO_3$/Graphene oxide composites with improved photocatalytic activity and selectivity for NO_x removal, Appl. Surf. Sci. (2017), http://dx.doi.org/10.1016/j.apsusc.2017.06.056

NO_2 generation is monitored simultaneously during the photocatalytic oxidation of NO, and the result is shown in Fig. 8b. NO_2 generation in BOC is relatively high with a yield of 19.2 ppb NO_2 despite that the NO removal over BOC is the lowest among all samples. After compositing with GO (BOC–GO 1.0), the NO_2 concentration increased to 36.8 ppb. However, the NO_2 yield efficiency (NO_2 yield efficiency = $\frac{C_{NO_2}}{C_0 \text{ of } NO - C_{NO}} \times 100\%$) almost remains the same in BOC and BOC–GO 1.0 samples, showing the efficiency of 40.6% and 41.3%, respectively. This observation suggests that

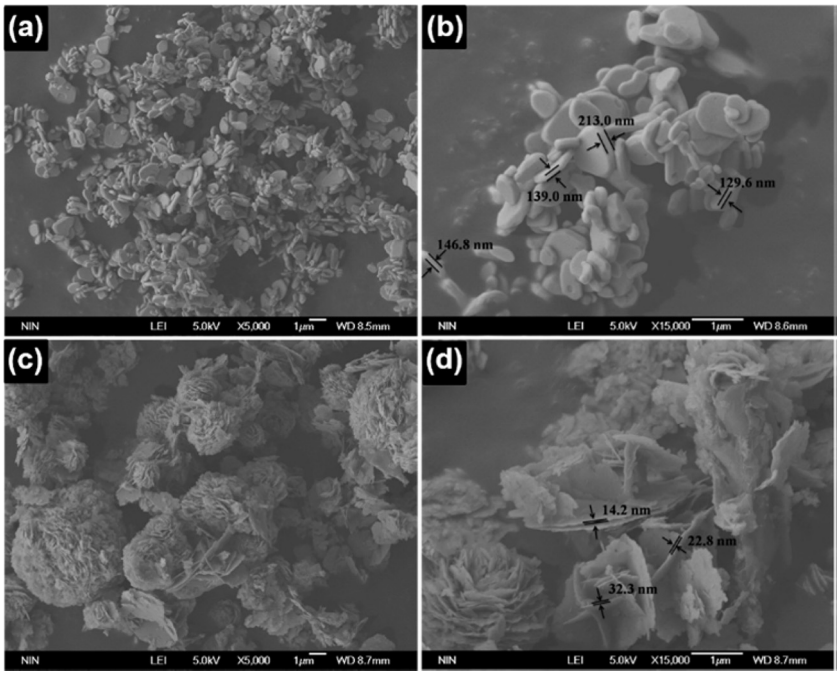

Fig. 5. SEM images of NBOC (a, b) and NBOC–GO 1.0 (c, d).

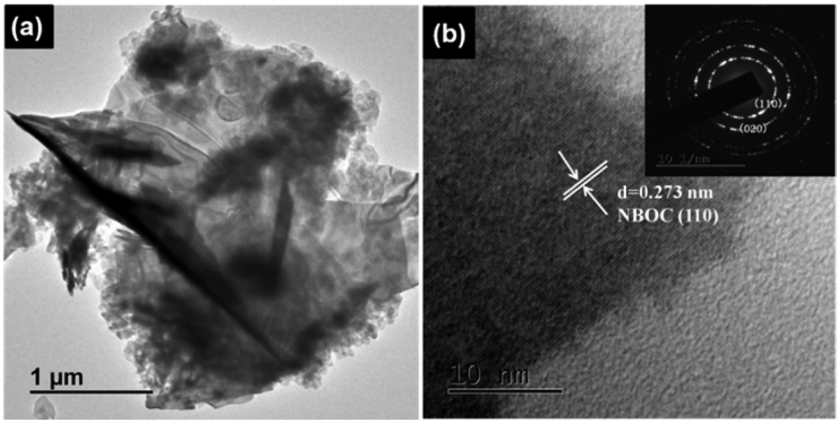

Fig. 6. Low magnification TEM image of (a) NBOC–GO 1.0, and (b) HRTEM of NBOC–GO 1.0, Inset: SEAD patterns of NBOC–GO 1.0.

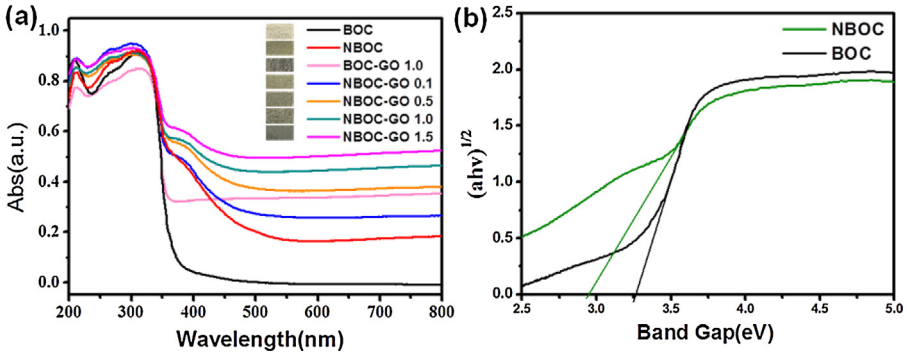

Fig. 7. (a) UV–vis diffuse reflectance spectra of pure BOC, NBOC, BOC-GO 1.0 and NBOC–GO composites and (b) the estimated band gap of BOC and NBOC.

Please cite this article in press as: M. Chen, et al., Visible-light-driven N-$(BiO)_2CO_3$/Graphene oxide composites with improved photocatalytic activity and selectivity for NO_x removal, Appl. Surf. Sci. (2017), http://dx.doi.org/10.1016/j.apsusc.2017.06.056

Table 1
Summary of surface area of pure BOC, BOC–GO 1.0, NBOC, and NBOC–GO composites.

Samples	BOC	BOC- GO 1.0	NBOC	NBOC-GO			
				0.1	0.5	1.0	1.5
BET Surface Area (m^2/g)	2.32	5.47	25.31	22.60	23.62	22.94	22.64

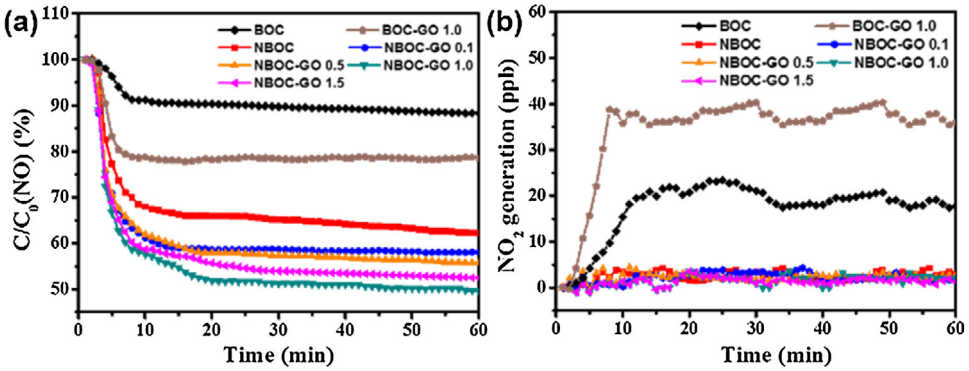

Fig. 8. (a) C/C_0 of NO vs. irradiation time, and (b) the NO_2 generation under visible-light irradiation.

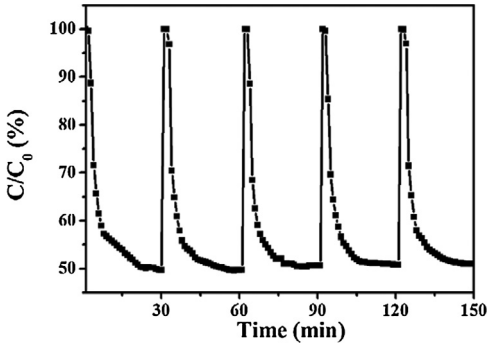

Fig. 9. Re-utilization test of NBOC–GO 1.0 photocatalyst under visible-light irradiation.

the GO shows ignorable effect for NO_2 generation. Interestingly, for the NBOC photocatalysis, the NO_2 concentration is lower than 2 ppb with a NO_2 yield efficiency of 0.5%, indicating that N doping plays a significant role of inhibiting the NO_2 generation. In all four NBOC–GO composites, the NO_2 generation concentrations maintain at equivalent levels to NBOC at a range of 1.6–3.0 ppb (with NO_2 yield efficiency at 0.4%–0.7%). This observation is in agreement with the conclusion that GO shows ignorable effect on the NO_2 yield efficiency regardless whether the GO content is changed or not. Herein, the NBOC–GO composite is a highly selective photocatalyst on inhibiting the NO_2 generation that completely benefits from the role of N doping.

In view of real application, the stability of photocatalyst is important during the photocatalytic reaction. The re-utilization experiment is conducted to test the stability of the optimum photocatalyst of NBOC–GO 1.0 sample. Fig. 9 shows that the decay rate of NO maintains a similar level after five consecutive cycles, suggesting that the obtained NBOC–GO 1.0 photocatalyst owns high stability and presents no photocorrosion within the test period.

3.5. Photocurrrent, electrochemical impedance spectroscopy, and photoluminescence spectra

The photocurrent response experiments are performed to investigate the interfacial charge separation and transfer dynamics of photoelectrons. Fig. 10a shows the photocurrent response of BOC, NBOC and NBOC–GO 1.0 electrodes under visible light irradiation. No photocurrent is generated on BOC sample under visible light irradiation because BOC is inert to visible light with its wide band gap [9]. In comparison, the NBOC shows the generation of photoexcited electrons under visible-light irradiation because the N doping explores the visible light response, which is in agreement with the diffuse reflectance spectroscopy (DRS) results. The higher photocurrent of NBOC–GO 1.0 than NBOC indicates a rapid photocurrent generation in the NBOC–GO 1.0 composite because GO facilitates the separation and migration of charge carriers, resulting from its role of electron acceptor and transfer channel [19,25].

EIS is used to assess the charge mobility of samples. In general, the increased charge mobility leads to the small EIS arc radius. Fig. 10b shows the EIS measurement results of BOC, NBOC and NBOC–GO 1.0 samples. The NBOC–GO 1.0 shows the smallest semicircle among the three samples, suggesting that the photogenerated e^-–h^+ pairs in the NBOC–GO composite is easily separated and transferred to the surface of sample.

The PL emission spectra of BOC, BOC–GO 1.0, NBOC and NBOC–GO 1.0 by the excitation wavelength at 280 nm are compared in Fig. 10c. The fluorescence emission peaks of all samples are mainly centered at 350–500 nm. The intensity follows the order BOC > BOC–GO 1.0 > NBOC > NBOC–GO 1.0. The lower the PL intensity, the higher the possibility of photoexcited charge-carrier separation [26]. The lower PL emission of NBOC than BOC indicates that the recombination emission in $(BiO)_2CO_3$ is reduced by N doping. Furthermore, the NBOC–GO 1.0 composite owns the lower PL emission intensity than NBOC because the high electrical conductivity of GO facilitates the charge separation and migration [27,28], thereby inhibiting the recombination of charge carries. In addition, the BOC–GO 1.0 composite shows higher PL intensity than NBOC, demonstrating that the N doping on $(BiO)_2CO_3$ is an efficient way to decrease the e^-–h^+ recombination compared with construction composite with GO.

3.6. Photocatalytic mechanism

In order to investigate the active radicals and evaluate the photoreaction mechanism, ESR spin-trap technique is used for the detection of $^{\bullet}OH$ and $^{\bullet}O_2^-$ radicals in BOC, NBOC and NBOC-GO samples under visible light irradiation. The seven antisymmetric peaks observed in NBOC and NBOC–GO 1.0 in Fig. 11a are ascribed to the $^{\bullet}OH$ radicals.[24] The four-line spectrum with an intensity ratio of 1:1:1:1 (Fig. 11b) are observed in NBOC and NBOC–GO 1.0, suggest-

Please cite this article in press as: M. Chen, et al., Visible-light-driven N-$(BiO)_2CO_3$/Graphene oxide composites with improved photocatalytic activity and selectivity for NO_x removal, Appl. Surf. Sci. (2017), http://dx.doi.org/10.1016/j.apsusc.2017.06.056

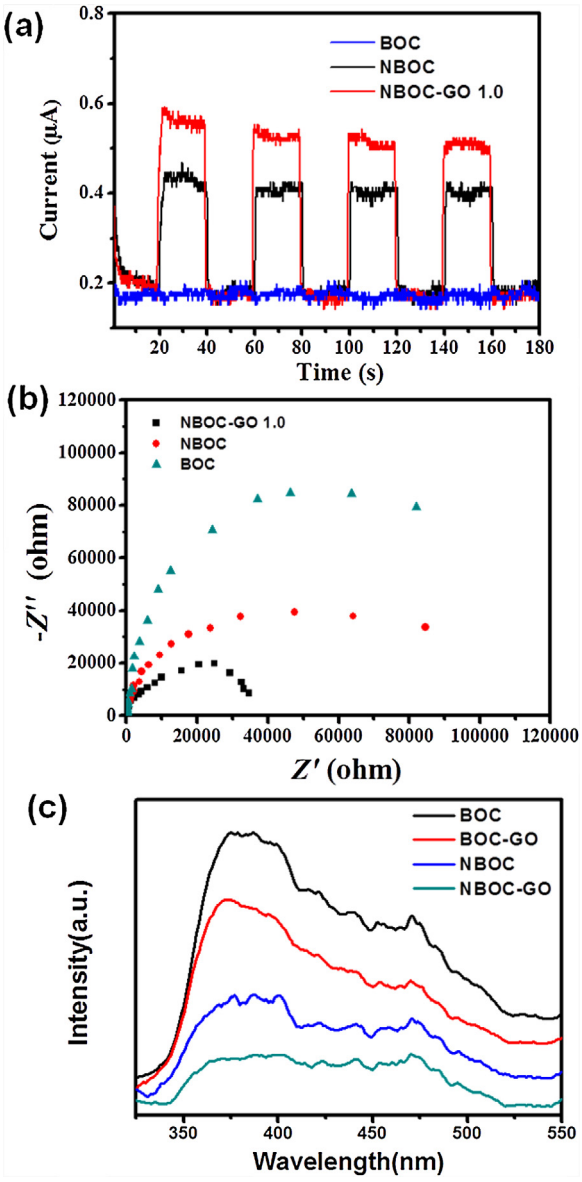

Fig. 10. (a) Photocurrent responses under visible-light irradiation, (b) electrochemical impedance spectroscopy measurements of BOC, NBOC and NBOC–GO 1.0, and (c) the PL spectrum of BOC, BOC–GO 1.0, NBOC, NBOC–GO 1.0 excited by 280 nm.

ing the presence of $^{\bullet}O_2^-$ radicals. These findings demonstrate that $^{\bullet}OH$ and $^{\bullet}O_2^-$ radicals are formed in both NBOC and NBOC–GO 1.0 samples under visible light irradiation. Moreover, the signal intensities of $^{\bullet}OH$ and $^{\bullet}O_2^-$ radicals over NBOC–GO 1.0 is higher than

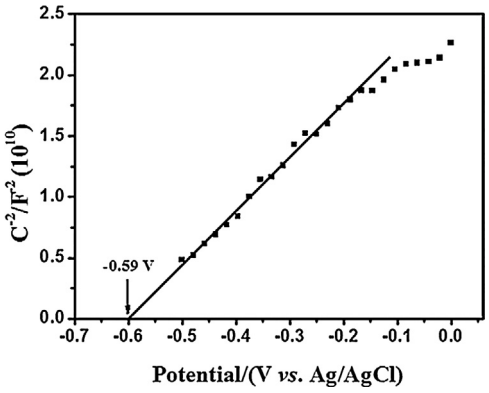

Fig. 12. Mott–Schottky plots of the NBOC.

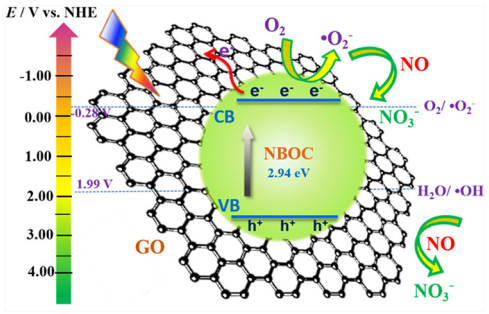

Fig. 13. Schematic of the photogenerated charge transfer in the NBOC–GO composite under visible-light irradiation.

NBOC, suggesting the generation of more radicals in NBOC–GO 1.0 composite. In addition, no DMPO–$^{\bullet}OH$ and DMPO–$^{\bullet}O_2^-$ signal is found in BOC, because the BOC photocatalyst (band gap of 3.26 eV) cannot be excited by the irradiation of visible light.

The Mott-Schottky measurements were carried out to estimate NBOC band edge positions. Fig. 12 shows the typical Mott–Schottky plots ($1/C^2$ versus voltage (V/SCE)) for the NBOC sample. It is clear seen that the capacitance decreases with the increase of applied potential for NBOC, which is in accordance with the behavior of *n*-type semiconductor. The flat band potential (V_{fb}) value of NBOC was estimated at −0.59 V versus Ag/AgCl at pH 7.0 (equivalent to −0.39 V vs. NHE at pH 7.0). Combined with the band gap (Eg = 2.94 eV) obtained from the DRS result, the relative position of band edges (CB/VB) is determined to be −0.39 V/2.55 V vs. NHE for NBOC. Fig. 13 shows a schematic of photogenerated charge transfer in the NBOC–GO composite. When the visible light irradiates on NBOC, the e^- and h^+ will be separated. The photogenerated h^+ from NBOC can oxidize the physically adsorbed H_2O to form $^{\bullet}OH$ radicals because the E_{VB} of NBOC (2.55) is more positive than the

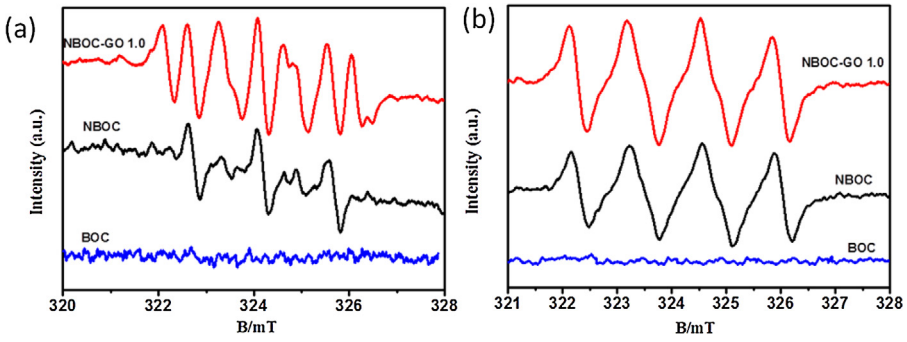

Fig. 11. Electron spin resonance spectra for (a) $^{\bullet}OH$ radicals and $^{\bullet}O_2^-$ radicals in BOC, NBOC and NBOC–GO 1.0 under visible-light irradiation.

Please cite this article in press as: M. Chen, et al., Visible-light-driven N-$(BiO)_2CO_3$/Graphene oxide composites with improved photocatalytic activity and selectivity for NO_x removal, Appl. Surf. Sci. (2017), http://dx.doi.org/10.1016/j.apsusc.2017.06.056

•OH/H_2O potential (1.99 V). Meanwhile, the E_{CB} of NBOC (-0.39 V) is more negative than $•O_2^-/O_2$ (−0.28 V). These analysis demonstrates that the •OH and $•O_2^-$ radicals involves in the photocatalysis processes over NBOC-GO composite. The photoreaction mechanism derived from the electronic band structure is agreement with the ESR results.

The better performance of NBOC–GO composites than NBOC should be ascribed to the following facts. First, the photo-absorber property of GO enables the wide photo-absorption of the NBOC–GO composites (as described in the DRS analysis), which contributes to a positive effect for the photocatalytic reaction [19]. Second, the superior electrical conductivity of GO facilities the photogenerated e^- transferring from the CB of NBOC to GO (Fig. 13). Thereby, the e^-–h^+ recombination is suppressed by the efficient electron acceptor and transfer channel roles of GO, leaving more h^+ charge carries and promoting the generation of •OH radicals. Third, the flower-like NBOC–GO microspheres assembled by thin nanosheets should benefit the photocatalytic performance by providing large exposure surface and facilitating the mobility of charge carries. In addition, N doping plays significant role on the enhanced photocatalytic activity and high selectivity, which should be ascribed to two reasons. First, this outcome is determined from DRS result. The useful light spectrum for photocatalytic reaction in NBOC (<600 nm) is broader than BOC (<400 nm). Second, the BET test in Table 1 showed that the S_{BET} of NBOC (25.3 m^2/g) is 11.9 times over BOC (2.3 m^2/g), which provides more active sites and more efficient transport pathways for reactants [9]. Thereby, the oxidations of NO and NO_2 are accelerated, leading to the improvement of NO removal and the inhibition of NO_2 generation.

4. Conclusions

A facile hydrothermal route for the synthesis of NBOC–GO composite is reported in this study, wherein the bismuth citrate (Bi source) is significant for NBOC formation. The optimum GO/NBOC ratio is determined as 1.0% in weight. The as-prepared NBOC–GO presents excellent NO removal efficiency and high selectivity with ignorable NO_2 generation. The excellent performance of NBOC–GO should be ascribed to the explored light absorption and large specific surface area from N doping, the photo absorber and electron acceptor role of GO, and the morphology modulation. N doping plays the crucial role in the NBOC–GO composite, which contributes to 74.6% of improvement in NO removal and full response for the inhibition of NO_2 generation.

Acknowledgments

This work is supported by the National Natural Science Foundation of China (grant numbers 41503102, 41573138, and 41401567) and the China Postdoctoral Science Foundation (grant number 2015M572568). Yu Huang is also supported by the "Hundred Talent Program" of the Chinese Academy of Sciences.

Appendix A. Supplementary data

Supplementary data associated with this article can be found, in the online version, at http://dx.doi.org/10.1016/j.apsusc.2017.06.056.

References

[1] A.A. Presto, M.A. Miracolo, N.M. Donahue, A.L. Robinson, Secondary organic aerosol formation from high-NO_x photo-oxidation of low volatility precursors: n-alkanes, Environ. Sci. Technol. 44 (2010) 2029–2034.
[2] D.G. Streets, S.T. Waldhoff, Present and future emissions of air pollutants in China: SO_2, NO_x, and CO, Atmos. Environ. 34 (2000) 363–374.
[3] H. Parlar, D. Angerhöfer, Verhalten von chemikalien in der umwelt, in: Chemische Ökotoxikologie, Springer, Berlin Heidelberg, 1995, pp. 3–124.
[4] D. Yang, S.H. Qi, N.L. Devi, F. Tian, Z.P. Huo, Q.Y. Zhu, J. Wang, Characterization of polycyclic aromatic hydrocarbons in PM2.5 and PM10 in tanggu district, tianjin binhai new area, China. Front. Earth Sci. 6 (2012) 324–330.
[5] K. Skalska, J.S. Miller, S. Ledakowicz, Trends in NO_x abatement: a review, Sci. Total Environ. 408 (2010) 3976–3989.
[6] M. Mansouri, H. Atashi, F.F. Tabrizi, G. Mansouri, N. Setareshenas, Fischer–Tropsch synthesis on cobalt–manganese nanocatalyst: studies on rate equations and operation conditions, Int. J. Ind. Chem. 5 (2014) 1–9.
[7] Y. Sun, Z. Zhao, F. Dong, W. Zhang, Mechanism of visible light photocatalytic NO_x oxidation with plasmonic Bi cocatalyst-enhanced $(BiO)_2CO_3$ hierarchical microspheres, Phys. Chem. Chem. Phys. 17 (2015) 10383–10390.
[8] F. Dong, Q. Li, Y. Zhou, Y. Sun, H. Zhang, Z. Wu, In situ decoration of plasmonic Ag nanocrystals on the surface of $(BiO)_2CO_3$ hierarchical microspheres for enhanced visible light photocatalysis, Dalton Trans. 43 (2014) 9468–9480.
[9] F. Dong, R. Wang, X.W. Li, W.K. Ho, Hydrothermal fabrication of N-doped (BiO)2CO3: structural and morphological influence on the visible light photocatalytic activity, Appl. Surf. Sci. 319 (2014) 256–264.
[10] Z.L. Ni, Y.J. Sun, Y.X. Zhang, F. Dong, Fabrication, modification and application of $(BiO)_2CO_3$-based photocatalysts: a review, Appl. Surf. Sci. 365 (2016) 314–335.
[11] H. Huang, X. Li, J. Wang, F. Dong, P.K. Chu, T. Zhang, Y. Zhang, Anionic group self-doping as a promising strategy: band-gap engineering and multi-functional applications of high-performance CO_3^{2-}-doped $Bi_2O_2CO_3$, ACS Catal. 5 (2015) 4094–4103.
[12] B. You, L. Wang, N. Li, C. Zheng, Improving the energy storage performance of graphene through insertion of pristine CNTs and ordered mesoporous carbon coating, ChemElectroChem 1 (2014) 772–778.
[13] P. Madhusudan, J. Yu, W. Wang, B. Cheng, G. Liu, Facile synthesis of novel hierarchical graphene-$Bi_2O_2CO_3$ composites with enhanced photocatalytic performance under visible light, Dalton Trans. 41 (2012) 14345–14353.
[14] D. Carr, O. von Ehrenstein, S. Weiland, C. Wagner, O. Wellie, T. Nicolai, E. von Mutius, Modeling annual benzene, yoluene, NO_2, and soot concentrations on the basis of road traffic characteristics, Environ. Res. 90 (2002) 111–118.
[15] Y. Zhou, Z. Zhao, F. Wang, K. Cao, D.E. Doronkin, F. Dong, J.-D. Grunwaldt, J. Facile, Synthesis of surface N-doped $Bi_2O_2CO_3$: origin of visible light photocatalytic activity and in situ DRIFTS studies, J. Hazard. Mater. 307 (2016) 163–172.
[16] B. You, L. Wang, L. Yao, J. Yang, Three dimensional N-doped graphene-CNT networks for supercapacitor, Chem. Commun. 49 (2013) 5016–5018.
[17] H. Lu, L. Xu, B. Wei, M. Zhang, H. Gao, W. Sun, Enhanced photosensitization process induced by the p–n junction of $Bi_2O_2CO_3$/BiOCl heterojunctions on the degradation of rhodamine B, Appl. Surf. Sci. 303 (2014) 360–366.
[18] H. Wang, Y.H. Liang, L. Liu, J.S. Hu, W.Q. Cui, Reduced graphene oxide wrapped Bi_2WO_6 hybrid with ultrafast charge separation and improved photoelectrocatalytic performance, Appl. Surf. Sci. 392 (2017) 51–60.
[19] H. Raj Pant, B. Pant, H. Joo Kim, A. Amarjargal, C. Hee Park, L.D. Tijing, E. Kyo Kim, C. Sang Kim, A green and facile one-pot synthesis of Ag–ZnO/RGO nanocomposite with effective photocatalytic activity for removal of organic pollutants, Ceram. Int. 39 (2013) 5083–5091.
[20] D. Wang, H. Jiang, X. Zong, Q. Xu, Y. Ma, G. Li, C. Li, Crystal facet Dependence of water oxidation on $BiVO_4$ sheets under visible light irradiation, Chem. Eur. J. 17 (2011) 1275–1282.
[21] P.Y. Dong, Y.H. Wang, B.C. Cao, S.Y. Xin, L.N. Guo, J. Zhang, F.H. Li, Ag_3PO_4/reduced graphite oxide sheets nanocomposites with highly enhanced visible light photocatalytic activity and stability, Appl. Catal. B 132–133 (2013) 45–53.
[22] D. Xu, B. Cheng, S. Cao, J. Yu, Enhanced photocatalytic activity and stability of Z-scheme Ag_2CrO_4-GO composite photocatalysts for organic pollutant degradation, Appl. Catal. B 164 (2015) 380–388.
[23] U. Holzwarth, N. Gibson, The Scherrer equation versus the 'Debye-Scherrer equation', Nat. Nano. 6 (2011) 534.
[24] Y.J. Chen, G.H. Tian, G.J. Man, R. Li, Y.T. Xiao, T.R. Han, Facile synthesis of well-dispersed Bi_2S_3 nanoparticles on reduced graphene oxide and enhanced photocatalytic activity, Appl. Surf. Sci. 378 (2016) 231–238.
[25] G. Li, D. Zhang, J.C. Yu, M.K.H. Leung, An efficient bismuth tungstate visible-light-driven photocatalyst for breaking down nitric oxide, Environ. Sci. Technol. 44 (2010) 4276–4281.
[26] H. Huang, J. Wang, F. Dong, Y. Guo, N. Tian, Y. Zhang, T. Zhang, Highly efficient $Bi_2O_2CO_3$ single-crystal lamellas with dominantly exposed {001} facets, Cryst. Growth Des. 15 (2015) 534–537.
[27] L. Chen, F. Chen, Y. Shi, J. Zhang, Preparation and visible light photocatalytic activity of a graphite-like carbonaceous surface modified TiO_2 photocatalyst, J. Phys. Chem. C 116 (2012) 8579–8586.
[28] X. Li, J.G. Yu, S. Wageh, Ahmed A. Al-Ghamdi, J. Xie, Graphene in photocatalysis: a review, Small 12 (2016) 6640–6696.

Please cite this article in press as: M. Chen, et al., Visible-light-driven N-$(BiO)_2CO_3$/Graphene oxide composites with improved photocatalytic activity and selectivity for NO_x removal, Appl. Surf. Sci. (2017), http://dx.doi.org/10.1016/j.apsusc.2017.06.056